ACS Catalysis

Review

pubs.acs.org/acscatalysis

# Selective Dehydration of Alkanediols into Unsaturated Alcohols over Rare Earth Oxide Catalysts

Satoshi Sato,* Fumiya Sato, Hiroshi Gotoh, and Yasuhiro Yamada

Graduate School of Engineering, Chiba University, Yayoi, Inage, Chiba, Japan 263-8522

Supporting Information

**ABSTRACT:** Syntheses of unsaturated alcohols in the vapor-phase catalytic dehydration of alkanediols over rare earth oxides are reviewed. $CeO_2$ effectively catalyzes the dehydration of 1,3-butanediol to produce 3-buten-2-ol and *trans*-2-buten-1-ol. Heavy rare earth oxides such as $Er_2O_3$, $Yb_2O_3$, and $Lu_2O_3$ selectively catalyze the dehydration of 1,4-butanediol to produce 3-buten-1-ol. In the dehydration of 1,5-pentanediol, $Yb_2O_3$, $Lu_2O_3$, and $Sc_{0.5}Yb_{1.5}O_3$ catalysts efficiently work to produce 4-penten-1-ol. The active and selective oxides are composed of large particles with well-crystallized fluorite or bixbyite structure. Small oxide particles with poor crystallinity decrease the selectivity to unsaturated alcohols because of their dehydrogenation ability. In the reactions of different alkanediols, the reactivity of alkanediol depends on the length between the OH groups as well as on the geometry of the catalyst surface, which is affected by the distance between rare earth cations. For example, over $CeO_2$, the reactivity order of the alkanediols is 1,3-butanediol > 1,4-butanediol > 1,5-pentanediol > 1,6-hexanediol. Quantum calculations support a probable reaction mechanism: OH groups and the H of the position-2 methylene group of 1,3-butanediol are interacted with the surface $Ce^{4+}$ to form a tridentate coordination, and the abstraction of the position-2 H by $Ce^{4+}$ is the initial step of 1,3-butanediol dehydration in the formation of unsaturated alcohols.

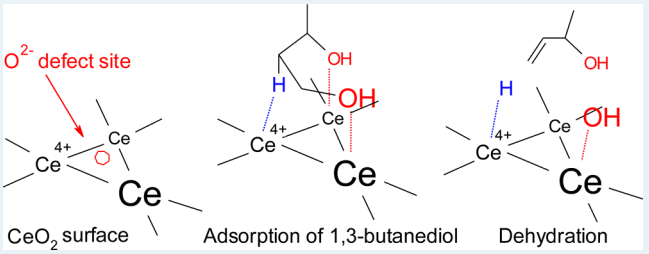


**KEYWORDS:** *unsaturated alcohol, dehydration, alkanediol, rare earth oxide, ceria, surface oxygen defects, nanorod*

## 1. CONVENTIONAL SYNTHESIS OF UNSATURATED ALCOHOL

Unsaturated alcohols are raw materials for important chemicals such as medicines, agricultural chemicals, perfumes, and polymers. In this review, production of unsaturated alcohols in the dehydration of alkanediols is a major object. Prior to the dehydration of alkanediols, various methods to produce unsaturated alcohols reported in patent literatures are briefly summarized. The processes are classified into six categories, depending on the reactions: (1) addition of formaldehyde to an olefin; (2) isomerization of an unsaturated epoxide; (3) oxidation of an olefin, followed by hydrolysis; (4) reduction of an unsaturated carbonyl compound; (5) esterification of an allyl halide, followed by saponification; and (6) decomposition of an alkanediol monocarboxylate, that is, monoesterification of $\alpha,\omega$-alkanediols with a carboxylic acid, followed by decomposition. The examples are introduced as follows:

**(1). Addition of Formaldehyde to an Olefin.** Brace reported that polymeric formaldehyde and liquid propylene were sealed and heated at 246 °C and an autogenic pressure of 100 MPa to produce 3-buten-1-ol, whereas a mixture of formaldehyde and isobutene also produced 3-methyl-3-buten-1-ol.[1] Heinemann et al., Bayer Aktiengesellschaft, Germany, reported 3-buten-1-ol production by adding formaldehyde to an olefin at a nitrogen pressure of 15 MPa (Figure 1).[2] The conversion is as low as 36% for 12 h. Nagareda et al., Kuraray Co. Ltd., Japan, reported synthesis of 3-methyl-3-buten-1-ol

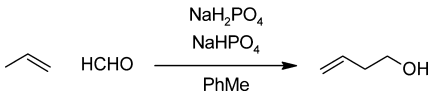


**Figure 1.** Preparation of 3-buten-1-ol by reacting formaldehyde with propene.[2]

from isobutene and formaldehyde with a metal tetrachloride (Figure 2).[3] This reaction requires a cosolvent, such as

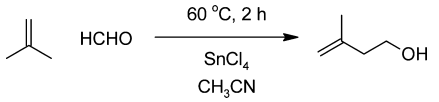


**Figure 2.** Synthesis of 3-methyl-3-buten-1-ol from isobutene and formaldehyde.[3]

acetonitrile and 1-propanol,[4] which dissolves both isobutene and a formaldehyde aqueous solution. The use of a cosolvent is questionable from the viewpoint of green chemistry.

**(2). Isomerization of Unsaturated Epoxide.** Tsuji et al. reported 3-buten-1-ol with a yield of 85% was produced in the rearrangement of 3,4-epoxy-1-butene using homogeneous Pd catalyst.[5] Falling (Eastman Chemical Company, Kingsport,

Received: December 3, 2012
Revised: February 25, 2013
Published: February 26, 2013

   dx.doi.org/10.1021/cs300781v | ACS Catal. 2013, 3, 721−734

TN) reported catalytic production of 3-buten-1-ol from 3,4-epoxy-1-butene and formic acid with a palladium catalyst. Although the yield of 3-buten-1-ol achieves a high value (78.5%), formic acid has a toxic and corrosive nature (Figure 3).[6] Falling also reported the hydrogenation of epoxy alkenes to

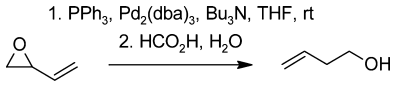


**Figure 3.** Catalytic production of 3-buten-1-ol from 3,4-epoxy-1-butene and formic acid.[6]

produce unsaturated alcohols. Both internal (74% yield of trans and cis mixture) and external olefins (23% yield) are produced (Figure 4).[7]

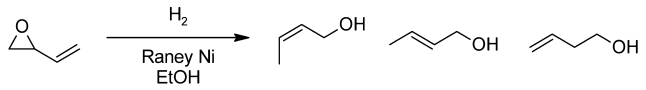


**Figure 4.** Hydrogenation of epoxy alkene.[7]

**(3). Oxidation of an Olefin, Followed by Hydrolysis.** Konishi and Matsufuji (Asahi Kasei Chemicals Co., Japan) reported oxidative conversion of 1-octene to 1-octene-3-ol: 15% of 1-octene is converted with high selectivity to 1-octen-3-ol (67%). Care should be exercised in this process because *tert*-butyl hydroperoxide is explosive (Figure 5).[8]

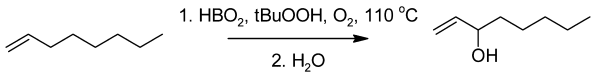


**Figure 5.** Synthesis of 1-octen-3-ol from 1-octene.[8]

**(4). Reduction of an Unsaturated Carbonyl Compound.** Several groups reported reduction of unsaturated aldehydes to allylic alcohols. In the reaction of citral to geraniol and citronellol, a high hydrogen pressure is required using ruthenium catalyst (Figure 6).[9,10] Kaneda and Mizugaki investigated hydrogenation of $\alpha,\beta$-unsaturated aldehyde in hydrogen and carbon dioxide: 95% of cynnamaldehyde was hydrogenated to cynnamyl alcohol (Figure 7).[11] Murzin et al. have reviewed the chemoselective hydrogenation of carbonyl compounds over heterogeneous catalysts.[12] NiSn alloy catalyzes the selective liquid-phase hydrogenation of $\alpha,\beta$-unsaturated carbonyl compounds to unsaturated alcohol.[13]

**(5). Esterification of an Allyl Halide and Saponification Reaction.** Oku and Yoshida (Nippon Shokubai Co. Ltd., Japan) reported novel synthesis process of 2-methy-2-propen-1-ol from 2-chloromethlylpropene by esterification, followed by saponification. In this process, an equivalent amount of sodium chloride is produced as a byproduct (Figure 8).[14]

**(6). Monoesterification of Alkanediols, Followed by Decomposition.** Yamanaka and Imai (Takasago Perfumery Co. Ltd., Japan) reported that 9-decen-1-ol with a yield of 80% and a selectivity of 89% is synthesized from 1,10-decanediol using monoesters of saturated fatty acids, such as palmitic acid

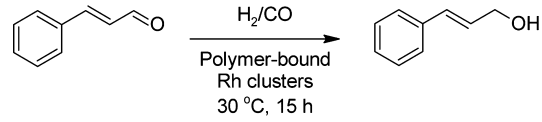


**Figure 7.** Hydrogenation of $\alpha,\beta$-unsaturated aldehyde in $H_2$ and CO.[11]

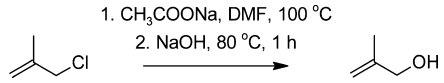


**Figure 8.** Synthesis of 2-methy-2-propen-1-ol from 2-chloromethlylpropene.[14]

and stearic acid, as catalysts in the vapor phase at temperatures of 330−350 °C (Figure 9).[15] 3-Buten-1-ol, however, is

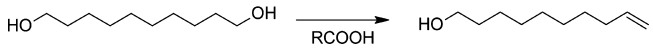


**Figure 9.** Synthesis of 9-decen-1-ol from 1,10-decanediol.[15]

produced with a yield of 50% and a selectivity of 59% in the dehydration of 1,4-butanediol, and tetrahydrofuran (THF) is produced as a byproduct. In contrast to the carboxylic acid-assisted dehydration, in the following sections, direct catalytic dehydration of alkanediols is introduced, with a focus on our recent research using oxide catalysts.

## 2. DEHYDRATION OF ALKANEDIOLS OVER ACIDIC CATALYSTS

**2.1. Dehydration of 1,3-Butanediol.** 1,3-Butanediol is widely used in cosmetics, such as a moisturizing agent. In the dehydration of 1,3-butanediol (compound **1** in Figure 10) catalyzed by acids, it is predicted that a reactive secondary OH group of position 3 is readily dehydrated to produce 2-buten-1-ol (**3** in Figure 10), according to the Sayzeff rule. However, acidic solids, such as silica−alumina, alumina, titania, and zirconia, produce a wide variety of products, described in Figure 10.[16,17] For example, over alumina catalyst at 250 °C, 1,3-butanediol is decomposed to formaldehyde, which is further acetalized with another reactant, 1,3-butanediol, to form 2-methyl-1,3-dioxane (**7** in Figure 10). Over titania and zirconia at 350 °C, 1,3-butanediol is decomposed to produce acetaldehyde and acetone. The expected 2-buten-1-ol is not produced because it is further dehydrated into 1,3-butadiene. Over silica−alumina at 250 °C, the major product is 1,3-butadiene, with a small amount of 3-buten-1-ol (**4** in Figure 10), which remains, as a result of its reactivity being lower than other unsaturated alcohols, **2** and **3**. Therefore, it is difficult to produce a specific unsaturated alcohol in the acid-catalyzed dehydration of 1,3-butanediol. Over the weak basic $CeO_2$ at 325 °C, however, 3-buten-2-ol (**2**) and *trans*-2-buten-1-ol (**3**) are produced with selectivities of 58% and 37%, respectively.[17]

**2.2. Dehydration of 1,4-Butanediol.** Figure 11 summarizes the acid-catalyzed dehydration of 1,4-butanediol.[18] $Al_2O_3$ and $SiO_2$−$Al_2O_3$ are active for the production of THF at temperatures higher than 200 °C. $Al_2O_3$ selectively catalyzes cyclodehydration to produce THF at 275 °C. Unsaturated

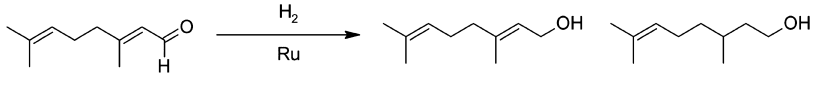


**Figure 6.** Reduction of citral to geraniol and citronellol.[9,10]


dx.doi.org/10.1021/cs300781v | ACS Catal. 2013, 3, 721−734

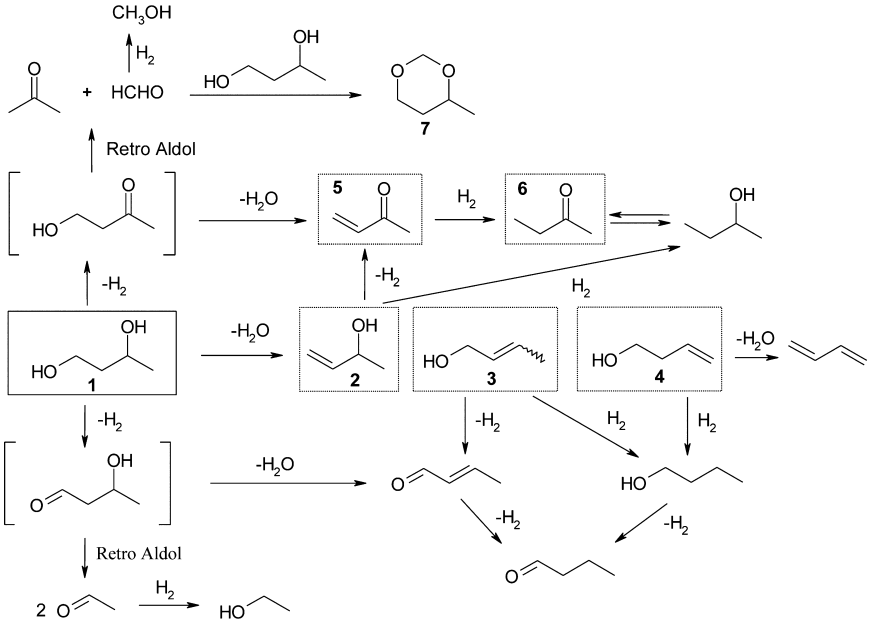


**Figure 10.** Acid-catalyzed decomposition of 1,3-butanediol.[16]

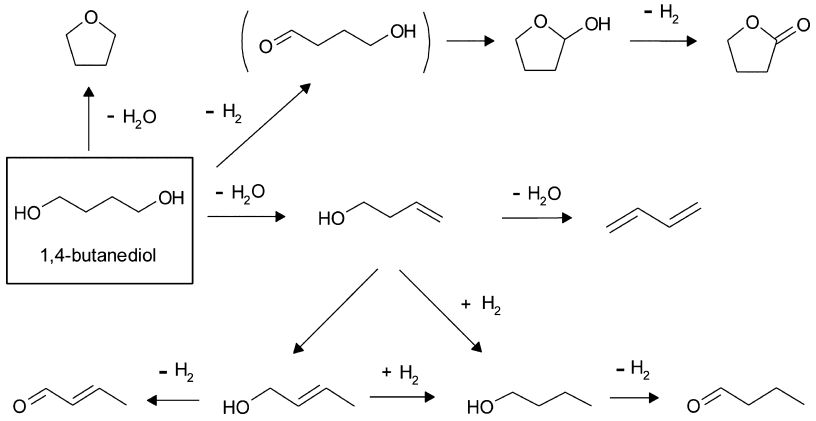


**Figure 11.** Acid-catalyzed decomposition of 1,4-butanediol.[18]

alcohols such as 3-buten-1-ol are rarely observed at 200−425 °C. Over $Al_2O_3$ and $SiO_2$−$Al_2O_3$, gaseous hydrocarbons, such as 1,3-butadiene, are observed in the reaction effluent. Other oxides, such as MgO and $ZrO_2$, are less active at 275 °C. Over $ZrO_2$ with the monoclinic crystal phase, THF is competitively produced, together with 3-buten-1-ol at 300−375 °C, and the yield of both THF and 3-buten-1-ol increase with increasing the contact time.[19] Formation of byproducts such as 2-buten-1-ol, 2-butenal, and 1-butanol is suppressed over monoclinic $ZrO_2$ at 325 °C. In liquid-phase dehydration, 1,4-butanediol is selectively cyclized to THF over solid acids, such as a cation exchange resin[20] and heteropolyacids.[21]

Over $CeO_2$, 1,4-butanediol is dehydrated to 3-buten-1-ol at 425 °C. $CeO_2$ shows a selectivity to 3-buten-1-ol of 55.8 mol %, with a small amount of 1,3-butadiene and THF at 425 °C. 2-Buten-1-ol, 2-butenal, 1-butanol, butanal, 2-hydroxytetrahydrofuran, and γ-butyrolactone are produced as byproducts. The initial product, 3-buten-1-ol, is isomerized, dehydrogenated, and hydrogenated, and 1,4-butanediol is also dehydrogenated and cyclized into γ-butyrolactone. When 1,4-butanediol is dehydrogenated initially, the resulting aldehyde, such as 4-hydroxybutanal, is readily hemiacetalized into 2-hydroxytetrahydrofuran, followed by dehydrogenation to γ-butyrolactone.[22]

## 3. SURFACE STRUCTURE OF RARE EARTH OXIDES

There are four types of crystal phases, such as hexagonal (H), monoclinic (M), cubic fluorite phase ($C_F$), and cubic bixbyite phase (C) in the rare earth oxides. The hexagonal phase is termed A-type; monoclinic phase, B-type; and cubic bixbyite phase, C-type.[23] We used different crystal structures of rare earth oxide samples calcined at different temperatures. The crystal structures depend on the element: $La_2O_3$, H; $CeO_2$, $C_F$; $Pr_6O_{11}$, $C_F$; $Nd_2O_3$, H; $Sm_2O_3$, M; $Eu_2O_3$, M; $Gd_2O_3$, M; $Tb_4O_7$, $C_F$; $Dy_2O_3$, C; $Ho_2O_3$, C; $Y_2O_3$, C; $Er_2O_3$, C; $Tm_2O_3$, C; $Yb_2O_3$, C; $Lu_2O_3$, C; and $Sc_2O_3$, C at calcination temperature of 1000 °C,[24] where this order is a decreasing order of the ionic radius of the rare earth cation, as cited in reference 25.

**3.1. Surface Structure of $CeO_2$.** It is well known that $CeO_2$ consists of the cubic fluorite phase (Figure 12). The crystal structure of $CeO_2$ is cubic fluorite where $Ce^{4+}$ has a coordination number 8, and $O^{2-}$ has the number 4. Since the {111} facet of $CeO_2$ is more stable than other facets, such as


dx.doi.org/10.1021/cs300781v | ACS Catal. 2013, 3, 721−734

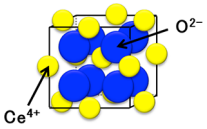


**Figure 12.** Unit cell of cubic fluorite $CeO_2$.[39]

{200} and {220},[26] the {111} facet becomes predominant with increasing calcination temperature.[27,28] Transmission electron microscope (TEM) observation reveals that the {111} facets are preferentially exposed on the surface of a large $CeO_2$ crystallite,[29] as shown in the model particles of Figure 13. The

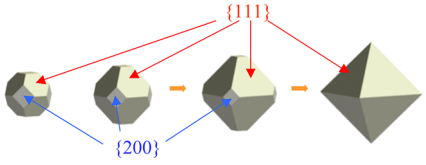


**Figure 13.** Change in morphology with crystal growth at high temperatures.[26,27]

surface of a $CeO_2$ (111) single crystal with oxygen defects has been observed microscopically.[30−34] Multiple defects with linear and triangular forms are rarely observed on the surface at an oxygen defect concentration of $<1 \times 10^{13}$ $cm^{-2}$, and a point defect site is preferable in the low concentration range of oxygen defects.[33] The model surface of the $CeO_2$ (111) plane is displayed in Figure 14. On the $CeO_2$ (111) surface, the number

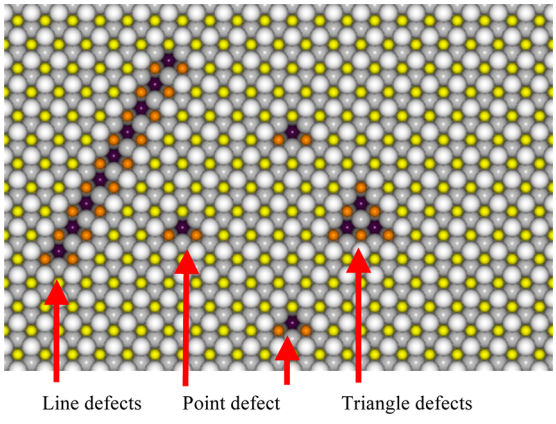


**Figure 14.** Model of $CeO_2$(111) surface with oxygen defects.[31−33] White large balls are on the top $O^{2-}$ layer; gray large ones are on the third $O^{2-}$ layer; yellow and orange ones are on the second Ce cation layers. Yellow indicates a 4+ cation and orange indicates a 3+ cation. Purple ones are on the forth $Ce^{4+}$ layer.

of surface oxygen defects decreases with increasing crystallite size.[35,36] The particles with low crystallinity contain many defects that would form multiple defects. The multiple defects, however, would expose reduced $Ce^{3+}$ ions[32] that would not participate in the redox cycle.

It has been reported that $CeO_2$, by nature, has oxygen defects, and the concentration of the oxygen defects depends on the crystallite size.[35,36] Kosacki et al. indicated that the concentration of oxygen defects decreases with $CeO_2$ crystalline growth because of the increase in the enthalpy for oxygen-defect formation with the growth.[35] Thus, it is reasonable that point oxygen-defect sites predominantly exist on the surface of $CeO_2$ at the reaction temperature. Here, there is a question whether a point defect site of $CeO_2$ (111) or a stoichiometric $CeO_2$ (111) surface provides the active sites in the dehydration of 1,3-butanediol. The answer to this question is addressed in Section 6.1.

**3.2. Surface Structure of Bixbyite Oxides.** The cubic bixbyite structure of rare earth sesqui oxide ($Ln_2O_3$) is related to the fluorite structure.[24,37,38] A subunit of bixbyite is the same as the unit cell of fluorite (Figure 12). The difference between the structures is that a subunit of bixbyite has two lattice $O^{2-}$ defects. Figure 15 shows four different subunits (octants I–

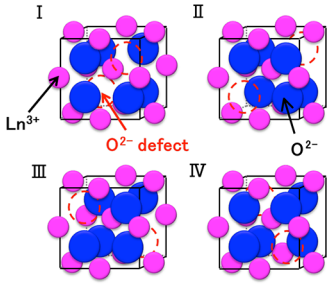


**Figure 15.** Subunits of cubic bixbyite phase ($Ln_2O_3$).[39]

IV).[39] The unit cell of cubic bixbyite phase regularly consists of eight subunits, as shown in Figure 16. Thus, the unit cell volume of cubic bixbyite is 8 times as large as that of fluorite.

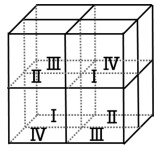


**Figure 16.** Unit cell of cubic bixbyite phase.[39] The numbers in the figure are the same as those in Figure 15.

The most stable facet of $CeO_2$ is the {111} plane,[26] as shown in Figure 13. In a cubic bixbyite phase, a {222} facet would be the most stable surface. In Figure 17, it is recognized that four

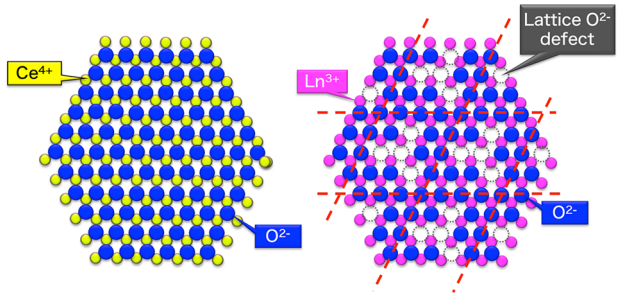


**Figure 17.** The {111} surface of $CeO_2$ (left) and the {222} surface of the cubic bixbyite phase (right).[39] A mirrored structure also exists in the bixbyite phase.

lattice $O^{2-}$ defects of a cubic bixbyite {222} facet are regularly located on the cubic fluorite {111} surface.[39] On the four $O^{2-}$ defects of cubic bixbyite {222} surface, three rare earth cations ($Ln^{3+}$) are located together with six other exposed $Ln^{3+}$ ions. Judging from TEM images of $Er_2O_3$,[24] the {222} facet grows with increasing calcination temperature, in analogy with the


dx.doi.org/10.1021/cs300781v | ACS Catal. 2013, 3, 721−734

$CeO_2$ {111} facet. In addition, $In_2O_3$ has the same crystal structure as bixbyite.[39,40]

## 4. DEHYDRATION OF ALKANEDIOLS TO UNSATURATED ALCOHOLS OVER $CEO_2$

**4.1. Dehydration of 1,3-Butanediols.** In our group, a series of research efforts on the dehydration of alkanediols have started from an important finding that 1,3-butanediol was dehydrated to produce two specific unsaturated alcohols, such as 3-buten-2-ol and *trans*-2-buten-1-ol in the vapor-phase, fixed-bed flow reactor over $CeO_2$ at 325 °C.[17] The catalytic dehydration is stable in the initial period of 5 h, and the recovered $CeO_2$ catalyst has the original color of yellow, indicating no coke formation. Figure 18 shows a scheme of the

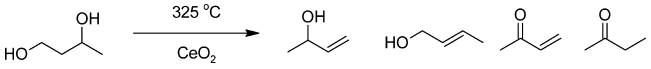


**Figure 18.** Dehydration of 1,3-butanediol over $CeO_2$.

dehydration of 1,3-butanediol to produce 3-buten-2-ol and *trans*-2-buten-1-ol with a small amount of byproducts, such as 3-buten-2-one, butanone *cis*-2-buten-1-ol, and 3-buten-1-ol over $CeO_2$.[17,27,28,41−43] The typical results of catalytic reactions over $CeO_2$ are listed, together with the results of other oxide catalysts, in Table 1.

In the dehydration of 1,3-butanediol, selectivity to the corresponding unsaturated alcohols is increased with increasing calcination temperature (Figure 19).[27,28] In $CeO_2$ calcined at temperatures as high as 1000 °C, both conversion and selectivity are higher than those at low temperatures. Since the experiment is performed at constant surface area, Figure 19 clearly indicates that large particles are more active and selective than the small ones. This suggests the importance of crystallinity of primary $CeO_2$ particles when considering the active surface of $CeO_2$.

In the dehydration of 1,3-butanediol, $CeO_2$ has a characteristic feature that the major products are 3-buten-2-ol and *trans*-2-buten-1-ol with few byproducts.[17] In the dehydration of symmetric molecules, such as 1,3-propanediol and 2,4-pentanediol, only 2-propen-1-ol and 3-penten-2-ol are formed as products, respectively.[41] In contrast, there exist much less reactive 1,3-alkanediols. 1,3-Alkanediols with an alkyl substituted on position 2, such as 2-methyl-1,3-propanediol, are less reactive than 1,3-diols without a position-2 alkyl group: the selectivity to 2-methyl-2-propen-1-ol decreases with the formation of 1-propanol and propanal via a C−C bond scission.[41]

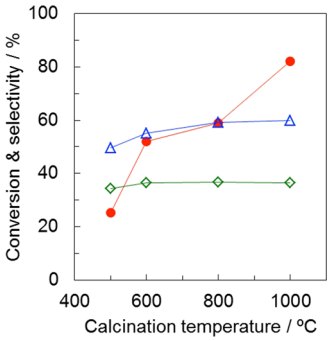


**Figure 19.** Changes in the conversion and selectivity with different calcination temperatures in the dehydration of 1,3-butanediol over $CeO_2$ at 325 °C.[28] Flow rate of 1,3-butanediol, $F$ = 6.5 cm$^3$ h$^{-1}$; reaction time, 2.5 h. (solid circle) Conversion, (open triangle) selectivity to 3-buten-2-ol, (open diamond) selectivity to 2-buten-1-ol. The surface area of the catalyst placed in the reactor is fixed at 21.1 m$^2$ with different loaded amounts of the catalysts.

**4.2. Dehydration of Other Alkanediols over $CeO_2$.** Our group has also investigated dehydration of several alkanediols to unsaturated alcohols over the $CeO_2$ catalyst.[41] Figure 20

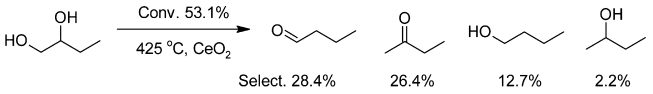


**Figure 20.** Dehydration of 1,2-butanediol over $CeO_2$.

shows the conversion and the selectivity in the vapor-phase dehydration of 1,2-butanediol at 425 °C. Unsaturated alcohol is not obtained from 1,2-butanediol; aldehyde and ketone are mainly produced. Figure 21 shows the dehydration of 1,2-propanediol. No unsaturated alcohol is produced, but saturated alcohols and carbonyl compounds are formed. Figure 22 shows the vapor-phase dehydration of 2,3-butanediol, which is mainly converted to 2-butanone, whereas 3-buten-2-ol is obtained with very small selectivity (2.7%). In the comparison of the reactivity

**Table 1. Examples of Vapor-Phase 1,3-Butanediol Dehydration over Various Catalysts at 325 °C**

| | | | | selectivity[a] (mol %) | | |
|---|---|---|---|---|---|---|
| catalyst[b] | SA[c] (m$^2$ g$^{-1}$) | cryst struct[d] | conv (%)[a,e] | 3-buten-2-ol | *trans*-2-buten-1-ol | ref |
| $La_2O_3$ (1000) | 6.8 | H | 2.4 | 7.1 | 1.9 | 43 |
| $CeO_2$ (500) | 141 | $C_F$ | 33.4[f] | 40.6 | 27.0 | 42 |
| $CeO_2$ (800) | 41.9 | $C_F$ | 32.9[f] | 54.1 | 35.7 | 42 |
| $CeO_2$ (1000) | 13.2 | $C_F$ | 72.6 | 58.0 | 35.7 | 43 |
| $Sm_2O_3$ (1000) | 6.4 | M | 3.1 | 11.5 | 4.0 | 43 |
| $Er_2O_3$ (500) | 33.5 | M | 23.8 | 29.4 | 14.7 | 43 |
| $Er_2O_3$ (800) | 21.5 | M + C | 24.9 | 46.6 | 29.0 | 43 |
| $Er_2O_3$ (1000) | 13.6 | C | 26.3 | 54.4 | 33.9 | 43 |
| $Yb_2O_3$ (1000) | 15.7 | C | 33.4 | 51.2 | 35.2 | 43 |
| $Lu_2O_3$ (1000) | 14.1 | C | 29.0 | 52.2 | 40.7 | 43 |
| $ZrO_2$ (as-received) | 100 | M | 25.3[g] | 16.3 | 18.7 | 16 |

[a]Conversion and selectivity were averaged in the initial 5 h. [b]The number in parentheses indicates calcination temperature of catalyst (°C). [c]SA, specific surface area. [d]Crystal structure: hexagonal (H), monoclinic (M), cubic fluorite ($C_F$), and cubic bixbyite (C). [e]$W/F$ = 0.15 g h cm$^{-3}$, where $W$ is catalyst weight (g) and $F$ is flow rate of liquid reactant (cm$^3$ h$^{-1}$). [f]$W/F$ = 0.05 g h cm$^{-3}$. [g]$W/F$ = 0.088 g h cm$^{-3}$.


dx.doi.org/10.1021/cs300781v | ACS Catal. 2013, 3, 721−734

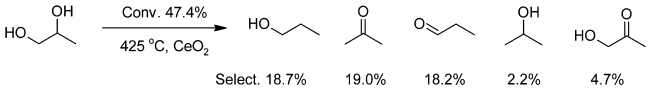


**Figure 21.** Dehydration of 1,2-propanediol over $CeO_2$.

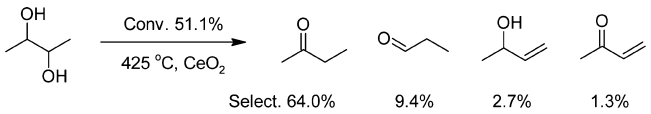


**Figure 22.** Dehydration of 2,3-butanediol over $CeO_2$.

of several butanediols over $CeO_2$, 1,2-, 2,3-, and 1,4-butanediol are less reactive than 1,3-butanediol. The dehydration of 1,4-butanediol over $CeO_2$ proceeds at 375 °C, which is the temperature higher than 325 °C that is required in the dehydration of 1,3-butanediol.[18]

Figure 23 shows the vapor-phase dehydration of 1,3-propanediol; 50.3% of 1,3-propanediol is converted with high

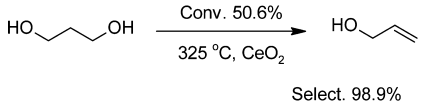


**Figure 23.** Dehydration of 1,3-propanediol over $CeO_2$.

selectivity of 2-propen-1-ol (98.9%) at 325 °C. A supported $CeO_2$ is also active in the dehydration of 1,3-propanediol. In patent literature, Kahn et al. (Lyondell Chemical Technology, L.P., USA) investigated the dehydration of 1,3-propanediol (Figure 23) over $CeO_2/\alpha$-$Al_2O_3$. Over $CeO_2/\alpha$-$Al_2O_3$, 82% of 1,3-propanediol was dehydrated with 75% selectivity to 2-propen-1-ol at 350 °C, whereas 60% of 1,3-propanediol was dehydrated with 70% selectivity to 2-propen-1-ol over $CeO_2/\gamma$-$Al_2O_3$.[44] Because the $CeO_2$-based catalysts were calcined at 500 °C during preparation in this case, the crystallinity of $CeO_2$ supported on $\alpha$-$Al_2O_3$ would be low. The selectivity to 2-propen-1-ol over the supported $CeO_2$ catalysts is expected to be improved: the selectivity could be increased if the catalyst is calcined at temperatures higher than 800 °C. Since pure $CeO_2$ calcined at 500 °C has low crystallinity and dehydrogenation ability to produce ketones from 1,3-butanediol, the low crystallinity resulted in the reduction of the selectivity to unsaturated alcohols (Table 1),[42] as shown in Figures 19 and 27.

Figure 24 shows the dehydration of 2,4-pentanediol, which is dehydrated to *trans*-3-penten-2-ol with a small amount of *cis*-3-

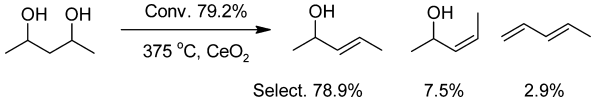


**Figure 24.** Dehydration of 2,4-pentanediol over $CeO_2$.

penten-2-ol.[41] Even at 425 °C, the selectivity to the completely dehydrated product, 1,3-pentanediene, is 8.3% at a conversion of 97%, whereas the selectivity to *trans*-3-penten-2-ol is 60.6%. Figure 25 shows the dehydration of 3-methyl-1,3-butanediol. Two unsaturated alcohols, 2-methyl-3-buten-2-ol and 3-methyl-2-buten-1-ol, are obtained from 3-methyl-1,3-butanediol.[41]

Figure 26 shows the dehydration of 1,4-butanediol to produce 3-buten-1-ol with byproducts such as THF and γ-

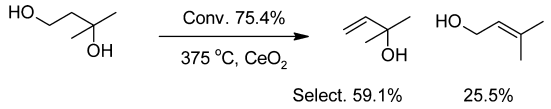


**Figure 25.** Dehydration of 3-methyl-1,3-butanediol over $CeO_2$.

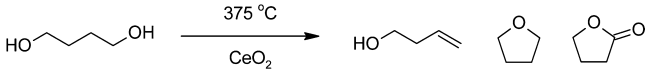


**Figure 26.** Dehydration of 1,4-butanediol over $CeO_2$.

butyrolactone.[41] The selectivity to 3-buten-1-ol exceeds 70% at 375 °C over $CeO_2$ calcined at 800 °C (Table 2).

In the dehydration of 1,4-butanediol, both the conversion and the selectivity to 3-buten-1-ol are increased with increasing calcination temperature (Figure 27).[27,28] This behavior is similar to that of 1,3-butanediol, shown in Figure 18. A similar dependency of calcination temperature on the catalytic activity of $CeO_2$ has been reported in the liquid-phase synthesis of dimethylcarbonate from methanol and carbon dioxide using $CeO_2$ catalysts calcined at different temperatures.[45]

Zhao et al. have also investigated the dehydration of 1,4-butanediol over $CeO_2$ with different morphologies.[46] They prepared three $CeO_2$ samples with different precipitation reagents, such as NaOH, $NH_4OH$, and $Na_2CO_3$. $CeO_2$ prepared with $Na_2CO_3$ mainly exposed the {111} facet; other $CeO_2$ catalysts exposed both the {111} and {200} facets. $CeO_2$ prepared with $Na_2CO_3$ showed high conversion and high selectivity to 3-buten-1-ol in the dehydration of 1,4-butanediol. It is confirmed that $CeO_2$ {111} facets have the active sites for the dehydration of butanediol into the corresponding unsaturated alcohols.

In the dehydration of 1,5-pentanediol over $CeO_2$, δ-valerolactone is a main product, together with 4-penten-1-ol and cyclopentanone (Figure 28).[47] The selectivity to 4-penten-1-ol is low (26.0% at 375 °C); therefore, $CeO_2$ is an inefficient catalyst in the dehydration of 1,5-pentanediol. In summary, the reactivity order of the alkanediols over $CeO_2$ is as follows: 1,3-butanediol > 1,4-butanediol > 1,5-pentanediol. In addition, it should be noted that 1,6-hexanediol is converted to cyclopentanone over $CeO_2$ with high selectivity via dehydrogenation followed by ketonization.[48] Therefore, it is summarized that $CeO_2$ specifically catalyzes the dehydration of 1,3-alkanediols to the corresponding unsaturated alcohols.

## 5. DEHYDRATION OF ALKANEDIOLS TO UNSATURATED ALCOHOLS OVER RARE EARTH OXIDES

As described in Section 3.2, cubic bixbyite oxides, such as $Er_2O_3$, $Yb_2O_3$, and $Lu_2O_3$, have the same crystal structure as $CeO_2$. Bixbyite oxide (222) surfaces with a astructure similar to the $CeO_2$ (111) surface (Figure 17) are expected to show high catalytic activity in the dehydration of alkanediols. As we had expected, the vapor-phase dehydration of alkanediol has proceeded over rare earth oxides with bixbyite structure.[43]

**5.1. Dehydration of 1,3-Butanediol over Rare Earth Oxides.** Table 1 also lists the conversion and the selectivity in the dehydration of 1,3-butanediol over several rare earth oxides at 325 °C. $CeO_2$ and heavy rare earth oxides, such as $Tb_4O_7$, $Dy_2O_3$, $Ho_2O_3$, $Y_2O_3$, $Er_2O_3$, $Tm_2O_3$, $Yb_2O_3$, $Lu_2O_3$, and $Sc_2O_3$, show high selectivity to 3-buten-2-ol and *trans*-2-buten-1-ol with a small amount of oxidized products, such as butanone, 3-


dx.doi.org/10.1021/cs300781v | ACS Catal. 2013, 3, 721−734

**Table 2. Examples of Vapor-Phase 1,4-Butanediol Dehydration over Various Catalysts**

| catalyst[a] | SA ($m^2$ $g^{-1}$) | temp (°C) | $W/F^b$ (g h $cm^{-3}$) | conv (%) | select (mol %) 3-buten-1-ol | THF | GBL[c] | ref |
|---|---|---|---|---|---|---|---|---|
| $La_2O_3$ (800) | 18 | 375 | 0.046 | 2.4 | 40.4 | 11.7 | 13.8 | 51 |
| $CeO_2$ (500) | 141 | 375 | 0.023 | 16.7 | 48.0 | 32.4 | 8.9 | 28 |
| $CeO_2$ (800) | 34 | 375 | 0.046 | 22.0 | 72.5 | 6.7 | 5.1 | 51 |
| $Sm_2O_3$ (800) | 20 | 375 | 0.046 | 5.0 | 59.2 | 25.9 | 6.6 | 51 |
| $Er_2O_3$ (800) | 22 | 375 | 0.046 | 30.2 | 85.9 | 5.3 | 0.8 | 51 |
| $Yb_2O_3$ (800) | 29 | 375 | 0.046 | 33.9 | 87.6 | 1.3 | 0.9 | 51 |
| $Lu_2O_3$ (800) | 28 | 375 | 0.046 | 36.7 | 83.6 | 2.3 | 0.4 | 51 |
| $In_2O_3$ (900) | 17.5 | 325 | 0.12 | 79.6 | 79.0 | 4.8 | 9.7 | 40 |
| tetragonal $ZrO_2$ (400) | 91 | 325 | 0.407 | 99.9 | 0.7 | 96.8 | 0.2 | 54 |
| monoclinic $ZrO_2$ (400) | 56 | 325 | 0.407 | 56.2 | 38.4 | 60.1 | 0.7 | 54 |
| 1.5 mol % Na/m-$ZrO_2$ (400) | 97 | 325 | 0.169 | 18.7 | 71.8 | 20.8 | 2.1 | 53 |
| 1.5 mol % Na/m-$ZrO_2$ (400) | 97 | 375 | 0.169 | 90.1 | 62.1 | 28.0 | | 53 |
| 10 wt % $Yb_2O_3$/m-$ZrO_2$ (400) | 40 | 325 | 0.407 | 50.8 | 86.5 | 4.3 | 1.1 | 54 |
| 10 wt % $Yb_2O_3$/m-$ZrO_2$ (800) | 37 | 325 | 0.407 | 73.1 | 85.4 | 12.1 | 0.7 | 54 |

[a]The number in parentheses indicates the calcination temperature of the catalyst (°C). m-$ZrO_2$ indicates monoclinic $ZrO_2$ [b]$W$ is the catalyst weight (g), and $F$ is the flow rate of the liquid reactant ($cm^3$ $h^{-1}$). [c]GBL = γ-butyrolactone.

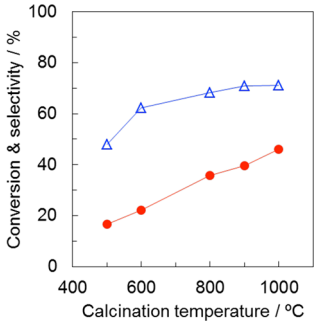


**Figure 27.** Changes in the conversion and selectivity with different calcination temperatures in the dehydration of 1,4-butanediol over $CeO_2$ at 375 °C. Flow rate of 1,4-butanediol, $F$ = 6.5 $cm^3$ $h^{-1}$; reaction time, 2.5 h. (Solid circle) Conversion, (open triangle) selectivity to 3-buten-1-ol. The surface area of the catalyst placed in the reactor is fixed at 21.1 $m^2$ with different loaded amounts of the catalyst.[28]

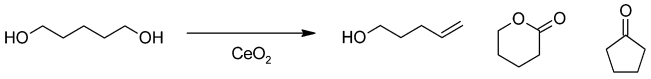


**Figure 28.** Dehydration of 1,5-pentanediol.

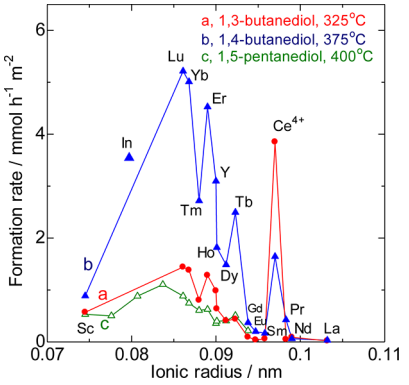


**Figure 29.** Changes in the formation rate of the unsaturated alcohols with ionic radius of rare earth cations. (a) 3-Buten-2-ol, 3-buten-1-ol, *cis*- and *trans*-2-buten-1-ol, in the dehydration of 1,3-butanediol over rare earth oxides (calcined at 1000 °C) at 325 °C.[43] (b) 3-Buten-1-ol in the dehydration of 1,4-butanediol over rare earth oxides (calcined at 1000 °C) at 375 °C.[51] (c) 4-Penten-1-ol in the dehydration of 1,5-pentanediol over rare earth oxides (calcined at 800 °C) at 400 °C.[55,57] The datum for $In_2O_3$ calcined at 900 °C is cited from ref 40.

buten-2-one, and propanone.[43,49] In contrast, except for $CeO_2$, light rare earth oxides, such as $La_2O_3$, $Pr_6O_{11}$, $Nd_2O_3$, $Sm_2O_3$, $Eu_2O_3$, and $Gd_2O_3$, mainly catalyze production of ketones such as butanone, 3-buten-2-one, and propanone. The calcination temperature also affects the catalytic activity of $Er_2O_3$, as realized in $CeO_2$ (Table 1). Calcination of $Er_2O_3$ at high temperature induces high selectivity to the unsaturated alcohols. In addition, $CeO_2$–$ZrO_2$, that is, $CeO_2$-supported $ZrO_2$ and $ZrO_2$-supported $CeO_2$, also show catalytic activity in the dehydration of 1,3-butanediol.[50]

Figure 29 depicts the relationship between the ionic radius of the rare earth cation and the formation rate of the unsaturated alcohols in the dehydration of 1,3-butanediol over rare earth oxides calcined at 1000 °C.[43] The formation rate of the unsaturated alcohols based on unit surface area represents the intrinsic catalytic activity of the rare earth oxide for the formation of the unsaturated alcohols. In the dehydration of 1,3-butanediol over heavy rare earth oxides calcined at 1000 °C, the formation rate of unsaturated alcohols is increased with decreasing ionic radius. $CeO_2$ is an exception: $CeO_2$ is the most active among the catalysts tested in the dehydration of 1,3-butandiol.

**5.2. Dehydration of 1,4-Butanediol over Rare Earth Oxides.** Table 2 summarizes the conversion and the selectivity in the dehydration of 1,4-butanediol over rare earth oxides calcined at 800 °C. The major product is 3-buten-1-ol, and the minor products are THF, γ-butyrolactone, and 2-buten-1-ol. 2-Buten-1-ol is produced by the isomerization of 3-buten-1-ol. Weak basic heavy rare earth oxides, such as $Er_2O_3$, $Tm_2O_3$, $Yb_2O_3$, $Lu_2O_3$, and $Y_2O_3$, show a selectivity to 3-buten-1-ol higher than 80 mol %, whereas strong basic light rare earth oxides, such as $La_2O_3$, $Pr_6O_{11}$, $Nd_2O_3$, $Sm_2O_3$, and $Eu_2O_3$, produced THF and γ-butyrolactone more than heavy rare earth oxides did. Heavy rare earth oxides exhibit different catalytic activities in the dehydration of 1,4-butanediol, depending on their crystal structures. C-type cubic oxides with bixbyite structure, such as $Er_2O_3$, $Tm_2O_3$, $Yb_2O_3$, $Lu_2O_3$, or $Y_2O_3$, selectively produce 3-buten-1-ol, whereas monoclinic B-type rare earth oxides are less active and less selective. In particular,


dx.doi.org/10.1021/cs300781v | ACS Catal. 2013, 3, 721–734

Table 3. Dehydration of 1,5-Pentanediol over Rare Earth Oxides at 400 °C[55]

| catalyst[a] | conversion,[b] (%) | selectivity[b] (mol %) | | |
|---|---|---|---|---|
| | | 4-penten-1-ol | tetrahydropyran | δ-valerolactone |
| $Sc_2O_3$ | 63.3 | 75.5 | 7.5 | 1.6 |
| $CeO_2$ | 22.4 | 25.8 | 3.9 | 21.0 |
| $Sm_2O_3$ | 18.0 | 42.2 | 13.8 | 15.6 |
| $Er_2O_3$ | 39.3 | 60.0 | 17.4 | 7.9 |
| $Yb_2O_3$ | 50.9 | 64.0 | 10.7 | 6.4 |
| $Lu_2O_3$ | 50.9 | 74.0 | 8.3 | 2.8 |
| $Sc_{0.5}Yb_{1.5}O_3$[c] | 62.8 | 80.8 | 3.7 | 0.3 |

[a]The catalysts were calcined at 800 °C. [b]Conversion and selectivity were averaged in the initial 5 h. $W/F$ = 0.167 g h cm$^{-3}$, where $W$ is catalyst weight (g) and $F$ is flow rate of liquid reactant (cm$^3$ h$^{-1}$). [c]Cited from ref [57]

$Er_2O_3$, $Yb_2O_3$, and $Lu_2O_3$ show the highest formation rate of 3-buten-1-ol. In a way similar to that of $CeO_2$ (Figure 27), calcination temperature strongly affects the selectivity: THF and γ-butyrolactone are reduced over $Er_2O_3$ calcined at a high temperature of 1000 °C.[51]

Figure 29 also depicts the relationship between the ionic radius of the rare earth cations and the formation rate of 3-buten-1-ol in the dehydration of 1,4-butanediol over rare earth oxides at 375 °C.[51,52] Rare earth oxides ranging from $Lu^{3+}$ (ionic radius 0.0861 nm) to $Tb^{3+}$ (0.0923 nm)—namely, $Lu_2O_3$, $Yb_2O_3$, $Er_2O_3$, $Y_2O_3$, $Tm_2O_3$, and $Tb_4O_7$—show high formation rates of 3-buten-1-ol with high selectivity. The intrinsic catalytic activities of cubic bixbyites such as $Er_2O_3$, $Yb_2O_3$, and $Lu_2O_3$ are the highest, and these are followed by $Tm_2O_3$ and $Y_2O_3$ with cubic bixbyite phase. Cubic fluorites, such as $CeO_2$ and $Tb_4O_7$, are less active than the cubic bixbyite oxides. It is obvious that monoclinic and hexagonal light rare earth oxides are much less active than cubic rare earth oxides. Except for $CeO_2$, the reactivity of 1,4-butanediol over rare earth oxides is similar to that of 1,3-butanediol in Figure 29. Considering the difference in the reaction temperatures between 325 and 375 °C, the reactivity of 1,4-butanediol could be almost the same as that of 1,3-butanediol over the cubic bixbyite oxides if the reactivity were compared at the same temperature. It should be noted that a factor determined by ionic radius of rare earth cations affects the catalytic activity.

**5.3. Dehydration of Alkanediols with Long Carbon Chains over Rare Earth Oxides.** Table 3 shows the conversion and the selectivity data in the dehydration of 1,5-pentanediol over rare earth oxides (Figure 28).[55] $Sc_2O_3$ and $Lu_2O_3$ show high conversion and selectivity to 4-penten-1-ol higher than 70%; therefore, $Sc_2O_3$ and $Lu_2O_3$ are effective catalysts in the dehydration of 1,5-pentanediol. However, there is no appropriate rare earth oxide with the lattice parameter value between 0.9845 nm of $Sc_2O_3$ and 1.0391 nm of $Lu_2O_3$, in which the lattice parameter is directly correlated with the ionic radius of the rare earth cation. It had been expected that these materials might have interesting features of the dehydration reactions.

Galceran et al. have prepared cubic scandium ytterbium mixed oxide $Sc_{2-x}Yb_xO_3$ ($x$ = 0–2) by the Pechini method.[56] $Sc_{2-x}Yb_xO_3$ has a cubic bixbyite phase, regardless of composition. Lattice parameters of $Sc_{2-x}Yb_xO_3$ samples are a function of the ytterbium content, and the lattice parameter is linearly increased from 0.9845 to 1.0435 nm with increasing $x$ from 0 to 2.0.[43] These mixed oxides can compensate for the missing bixbyite oxide catalysts.

In the dehydration of 1,5-pentanediol, scandium ytterbium mixed oxide $Sc_{0.5}Yb_{1.5}O_3$ was more active than simple rare earth oxides, such as $Sc_2O_3$, $Lu_2O_3$, and $Yb_2O_3$, and other mixed oxides $Sc_{1.0}Yb_{1.0}O_3$ and $Sc_{1.5}Yb_{0.5}O_3$ (Figure 29).[57] The selectivity to 4-penten-1-ol surpasses 80 mol % over the $Sc_{2-x}Yb_xO_3$ catalysts ($x$ = 0.5, 1.0, and 1.5). The highest formation rate of 4-penten-1-ol is obtained at $x$ = 1.5 and is affected by the lattice parameter of cubic bixbyite $Sc_{2-x}Yb_xO_3$. In the dehydration of 1,4-butanediol, however, $Tm_2O_3$ is the most active among the rare earth oxide catalysts.[57] The catalytic activities depend on their crystal structures, but it is not strongly correlated to specific surface area. In summary, the reactivity order of the alkanediols over bixbyite oxides, such as $Er_2O_3$, $Yb_2O_3$, and $Lu_2O_3$, is as follows: 1,3-butanediol = 1,4-butanediol > 1,5-pentanediol > 1,6-hexanediol.

We have also investigated the vapor-phase dehydration of a wide variety of alkanediols with long carbon chains, such as 1,6-hexanediol, 1,7-heptanediol, 1.8-octanediol, 1,9-nonanediol, 1,10-decanediol, and 1,12-dodecanediol.[58] Table 4 shows the catalytic activity of several rare earth oxides in the dehydration of 1,6-hexanediol. The rare earth oxide samples are calcined at 800 or 1000 °C. Among the catalysts compared in Table 4, $Sc_2O_3$ shows the highest selectivity in the dehydration of 1,6-hexanediol into 5-hexen-1-ol, and the conversion over $Sc_2O_3$ is higher than those over the other rare earth oxides. Although $Lu_2O_3$, $Yb_2O_3$, $Er_2O_3$, and $Y_2O_3$ have high selectivity to 3-buten-1-ol in the dehydration of 1,4-butanediol, as described in Section 5.2, they are less selective than $Sc_2O_3$ in the formation of 5-hexen-1-ol from 1,6-hexanediol. As shown in Table 4, several cyclic compounds, such as oxacycloheptane, cyclopentanone, and cyclopentanemethanol, are observed as by-products (Figure 30).

Table 4. Dehydration of 1,6-Hexanediol over Rare Earth Oxides at 350 °C[58,a]

| catalyst[b] | conv (%) | selectivity (mol %) | | |
|---|---|---|---|---|
| | | 5-hexen-1-ol | oxacycloheptanone | cyclohexanone |
| $Sc_2O_3$ (800) | 47.8 | 60.9 | 4.4 | 0 |
| $Y_2O_3$ (1000) | 20.0 | 26.3 | 8.4 | 2.4 |
| $CeO_2$ (800) | 45.2 | 4.8 | 4.3 | 25.2 |
| $Yb_2O_3$ (1000) | 29.8 | 17.6 | 11.7 | 2.5 |
| $Lu_2O_3$ (1000) | 32.9 | 32.2 | 9.9 | 2.8 |

[a]Conversion and selectivity were averaged in the initial 5 h. $W/F$ = 1.39 g h cm$^{-3}$, where $W$ and $F$ are the catalyst weight and the feed rate of reactant alkanediol, respectively. 1,6-Hexanediol dissolved in ethanol at 20 wt % was fed through the reactor top. $N_2$ carrier flow rate = 27 cm$^3$ min$^{-1}$. [b]The number in parentheses indicates calcination temperature of catalyst (°C).


dx.doi.org/10.1021/cs300781v | ACS Catal. 2013, 3, 721–734

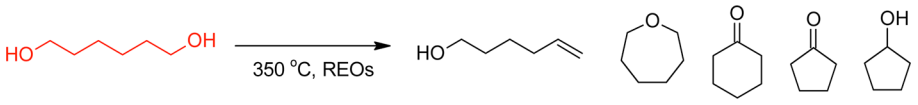


**Figure 30.** Dehydration of 1,6-hexanediol to 5-hexen-1-ol with byproducts such as oxacycloheptanone, cyclohexanone, cyclopentanone, and cyclopentanol.

In the vapor-phase dehydration of $\alpha,\omega$-alkanediols with long carbon chains over rare earth oxides, $Sc_2O_3$ shows the highest conversion and the highest selectivity to the corresponding unsaturated alcohol.[58] Figures 31−34 show the conversion and the selectivity to the corresponding unsaturated alcohol in the dehydration of $\alpha,\omega$-alkanediols over $Sc_2O_3$. Since the specific surface area of $Sc_2O_3$ is higher than 50 $m^2\ g^{-1}$, the conversion is high. However, the order of intrinsic activity of the rare earth oxides is similar to that in the dehydration of 1,4-butanediol in Figure 29: $Lu_2O_3$ is the most active among $Sc_2O_3$, $Y_2O_3$, $CeO_2$, $Yb_2O_3$, and $Lu_2O_3$,[58] and the selectivity to the corresponding unsaturated alcohols over $Sc_2O_3$ is the highest. Thus, the selectivity should be dependent on factors such as surface geometry and acid−base property.

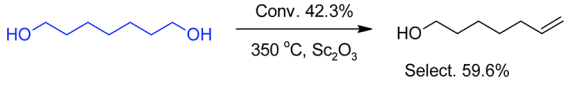


**Figure 31.** Dehydration of 1,7-heptanediol to 6-hepten-1-ol over $Sc_2O_3$.

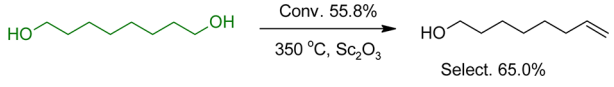


**Figure 32.** Dehydration of 1,8-octanediol to 7-octen-1-ol over $Sc_2O_3$.

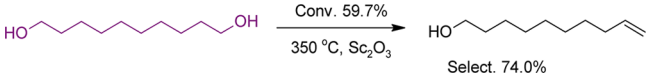


**Figure 33.** Dehydration of 1,10-decanediol to 9-decen-1-ol over $Sc_2O_3$.

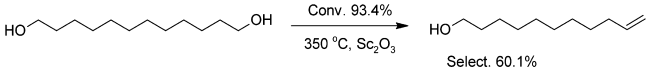


**Figure 34.** Dehydration of 1,12-dodecanediol to 11-dodecen-1-ol over $Sc_2O_3$.

## 6. DEHYDRATION MECHANISM OF ALKANEDIOLS OVER RARE EARTH OXIDES

**6.1. Mechanism of 1,3-Butanediol Dehydration over $CeO_2$.** Dehydration of a monoalcohol, such as 2-butanol, readily proceeds over acidic and basic catalysts.[59] In the acid- and base-catalyzed dehydration of alcohols, reaction should proceed via the E1 or E2 and E1cB mechanism, respectively. Rare earth oxides have Hofmann-elimination ability in the dehydration of 2-alcohols:[60−62] $\alpha$-Olefins, such as 1-butene, are formed with a selectivity higher than 80% in the dehydration of 2-butanol over rare earth oxides.[61] In the dehydration of 2-octanol over rare earth oxides, dehydrogenation to 2-octanone simultaneously proceeds with the formation of 1-octene:[62] the basic nature also affects the dehydrogenation. Rare earth oxides have attractive catalytic features, even in the reaction of monoalcohol. The dehydration of 1,3-butanediol over an acid and a base should produce 2-buten-1-ol (Sayzeff-elimination product) and 3-buten-1-ol (Hofmann-elimination product), respectively. Over acidic catalysts, however, various unsaturated alcohols are produced nonselectively because of isomerization (Figure 10). In the dehydration of 1,3-alkanediols over $CeO_2$ catalyst, however, it is difficult to explain the product selectivity through the simple mechanisms.

$CeO_2$ produces only 3-buten-2-ol and *trans*-2-buten-1-ol without producing 3-buten-1-ol. The product selectivity, however, cannot be explained by a simple acid-catalyzed mechanism via a carbocation. If an OH group on position 3 is eliminated first as an OH anion by an acidic site, 3-buten-1-ol has to be formed together with 2-buten-1-ol. We have considered a mechanism in the dehydration of 1,3-butanediol over $CeO_2$.[41] The $Ce^{4+}$−$Ce^{3+}$ redox nature of $CeO_2$ initially activates the hydrogen in position 2 of 1,3-butanediol, and the dehydration of 1,3-butanediols over $CeO_2$ follows a radical mechanism: a hydrogen atom located at position 2 is abstracted first, followed by the elimination of an OH radical (Figure 35).

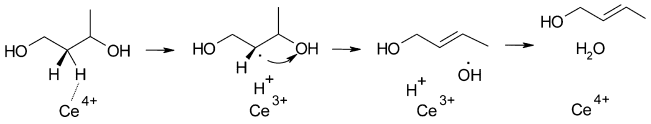


**Figure 35.** Possible radical mechanism of dehydration of 1,3-butanediol.[41]

Several results that support that the $Ce^{4+}$−$Ce^{3+}$ redox of $CeO_2$ contributes the abstraction of a hydrogen atom from the reactant are found in reactions such as alkylation of phenol[63] and ketonization of alcohol.[64] A surface $Ce^{4+}$ cation is reducible by the eliminated hydrogen radical in the catalytic cycle, and the eliminated OH radical is reduced by the $Ce^{3+}$, as shown in Figure 35. To realize the transition structure, the adsorption structure of alkanediols on $CeO_2$ is significant in the dehydration.

Density functional theory (DFT) and paired interacting orbital (PIO) calculations for the assumed adsorption model of 1,3-butanediol on a point oxygen-defect site of the $CeO_2$ (111) surface (Figure 13) are executed.[43,59,65,66] An adsorption structure of 1,3-butanediol is optimized on the point defect of $CeO_2$ (111) (Figure 36) from different starting geometries by DFT calculations. 1,3-Butanediol is activated by the adsorption with tridentate coordination. The bond lengths of $C^1$−$O^1$, $C^2$−$H^2$, and $C^3$−$O^3$ in 1,3-butanediol, where the number indicates the position of carbon atoms of the superscript, are increased in the optimized adsorption structure. Atomic orbital components in the PIO calculations reveal interactions between the 1,3-butanediol molecule and the point defect of $CeO_2$(111): an in-phase interaction between the O atoms in 1,3-butanediol and Ce cations, indicating that 1,3-butanediol is anchored by the interaction between two O atoms and two Ce cations, and out-of-phase interactions between $O^1$ and $C^1$ and between $H^2$ and $C^2$, induced by the in-phase interactions between $O^1$ and Ce and between $H^2$ and another


dx.doi.org/10.1021/cs300781v | ACS Catal. 2013, 3, 721−734

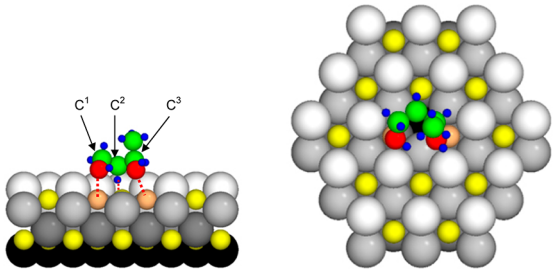


**Figure 36.** Adsorption model of 1,3-butanediol on $O^{2-}$ defect site of $CeO_2$(111). Left, side view; right, top view.[65] Green, red, and small blue balls represent C, O, and H atoms in 1,3-butanediol, respectively. At the $CeO_2$ surface layer, the first, third, fourth, and sixth layers are composed of $O^{2-}$, and the second and fifth layers, Ce cations. Small balls represent Ce cations; large ones mean $O^{2-}$; white large balls are on the top $O^{2-}$ layer; gray large ones are on the third $O^{2-}$ layer; yellow and orange ones are on the Ce layers. Yellow represents the 4+ cation and orange, the 3+ cation.

Ce, respectively, which result in the elongation of the $C^1-O^1$ and $C^2-H^2$ bonds.

The adsorption energy of 1,3-butanediol on the point defect site of the $CeO_2$ (111) surface is −102.7 kJ $mol^{-1}$ (Figure 37),

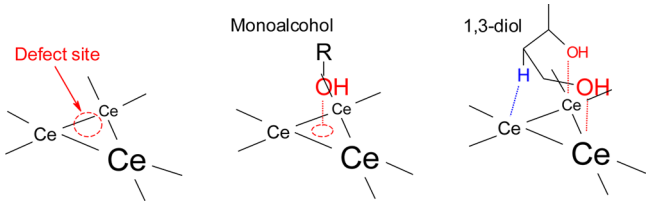


**Figure 37.** Image of adsorption of monoalcohol and 1,3-diol on an $O^{2-}$ defect site of $CeO_2$(111).[66]

which is more stable (by 20.0 kJ $mol^{-1}$) than that of 1,3-butanediol on the stoichiometric $CeO_2$ (111) surface, −82.7 kJ $mol^{-1}$. Thus, 1,3-butanediol preferentially adsorbs on the point defect site of the $CeO_2$ (111) surface and is dehydrated at the defect site. The adsorption energy of 1-butanol adsorbed on the point defect site is calculated to be −80.1 kJ $mol^{-1}$ (Figure 37). This is an important issue: adsorption of a monoalcohol, such as 2-buten-1-ol, which is a product, is less stable than that of 1,3-butanediol due to the single OH group coordinated to the defect site. Therefore, monoalcohols, including the unsaturated alcohols, cannot be reactants in the presence of 1,3-butanediol in the vapor phase.

The most probable reaction mechanism in the dehydration of 1,3-butanediols over $CeO_2$ is shown in Figure 38. Three Ce cations are exposed at a point $O^{2-}$ defect site of the $CeO_2$ (111) surface that provides an active center for the dehydration. Two oxygen atoms of the OH groups and one hydrogen atom of the position-2 methylene group in 1,3-butanediol interact with the three Ce cations. The hydrogen atom would be radically abstracted in the initial step, followed by the abstraction of one of the OH groups in 1,3-butanediol to produce only 3-buten-2-ol and 2-buten-1-ol.

The difference in the adsorption structure between monoalcohols and 1,3-alkanediols at the $O^{2-}$ defect site affects the difference in their reactivity: 1- and 2-butanols are less easily dehydrated than 1,3-butanediol over the $CeO_2$ surface.[41] In Section 3.1, it is stated that the $O^{2-}$ defect site could be the active center for the dehydration of 1,3-butanediols. The elimination of the position-2 H is the initial step in the dehydration of 1,3-butanediols: the $H^2$ atom of 1,3-butanediol is abstracted by a Ce cation.[65] Actually, the dehydration of monoalcohols rarely proceeds, and the monoalcohols are dehydrogenated to form carbonyl compounds at higher temperatures.[41] The $\beta$ H atom of a monoalcohol cannot access the Ce cations because the O atom of the OH group fills the defect site (Figure 37).[66] Therefore, unsaturated monoalcohols such as 2-buten-1-ol and 3-buten-2-ol are not dehydrated over $CeO_2$, so they are selectively produced in the reaction of 1,3-butanediols because of the suppression of stepwise dehydration to form dienes.

**6.2. Mechanism of 1,4-Butanediol Dehydration over Bixbyite-Type Oxides.** It is well-known that both acidic and basic sites exist on an oxide surface without neutralization. An acid−base concerted mechanism in the dehydration of alcohol over alumina is introduced.[67] The alumina surrounds the alcohol molecules, providing acid sites to act as proton donors or electron acceptors and basic sites to act as proton acceptors or electron donors. Setoyama has reviewed an industrial application of acid−base catalysis.[68] $NH_3$ and $CO_2$ can be used as a probe in the evaluation for acidic and basic sites.[69]

Temperature-programmed desorption of $NH_3$ did not reveal the acidic property of rare earth oxides because no clear adsorption is observed,[24] but $CO_2$ adsorbed on the samples. Thus, the surface of rare earth oxides is rather basic. To clarify the effects of acidic and basic sites of rare earth oxide catalysts on catalytic activity, vapor-phase dehydration of 1,3- and 1,4-butanediol was carried out under $NH_3$, $CO_2$, and $H_2$ flow conditions.[43,51] $NH_3$ could adsorb on acidic sites of rare earth oxides during the reaction, and $CO_2$ probably adsorbs on basic sites.

Table 5 summarizes the effects of poisoning gases on the conversion and the selectivity in the dehydration of 1,4-butanediol over $Er_2O_3$.[51] Under $NH_3$ and $CO_2$ flow conditions, the conversion and the selectivity to 3-buten-1-ol decrease. In particular, in $CO_2$, the conversion is one-half that in $N_2$ flow together with the reduction of the selectivity. The poisoning experiments indicate that both basic and acidic sites participate in the formation of 3-buten-1-ol via an acid−base concerted mechanism. The adsorption structure of 1,4-butanediol on a rare earth oxide catalyst is proposed.[51] The model adsorption

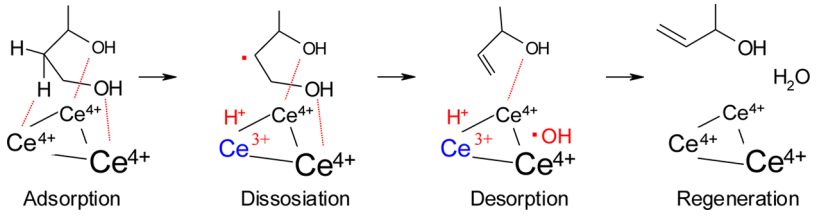


**Figure 38.** Probable reaction mechanism for the dehydration of 1,3-butanediol over $CeO_2$.[41]


dx.doi.org/10.1021/cs300781v | ACS Catal. 2013, 3, 721−734

**Table 5. Effect of Poisoning Gases on the Dehydration of 1,4-Butanediol over $Er_2O_3$ at 375 °C[51]**

| carrier gas[b] (flow rate/ $cm^3\ min^{-1}$) | conv[a] (%) | selectivity[a] (mol %) | | |
|---|---|---|---|---|
| | | 3-buten-1-ol | 2-buten-1-ol | THF + GBL[c] |
| $N_2$ (30) | 27.7 | 90.7 | 5.7 | 2.1 |
| $NH_3$+$N_2$ (15:15) | 18.7 | 86.9 | 5.6 | 3.9 |
| $CO_2$ (30) | 14.7 | 78.8 | 4.2 | 11.9 |

[a]Average conversion and selectivity in the initial 5 h. $W/F$ = 0.046 g h $cm^{-3}$, where $W$ is the catalyst weight (g) and $F$ is the flow rate of the liquid reactant ($cm^3\ h^{-1}$). [b]The catalyst was calcined at 1000 °C. [c]GBL, γ-butyrolactone.

structure of the active center is drawn in Figure 39. In analogy with an adsorption structure of alkanediol on the point defect

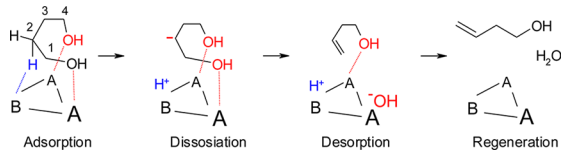


**Figure 39.** Probable reaction mechanism for the dehydration of 1,4-butanediol over bixbyite $Ln_2O_3$.[51] A and B represent acidic site and basic site, respectively.

site of $CeO_2$ (Figures 36–38),[41,65,66] we speculate that an active center is composed of two acidic sites and one basic site. It is reasonable that the OH groups of 1,4-butanediol adsorbs on acidic sites, and a position-2 hydrogen atom is activated by a basic site of heavy rare earth oxides (Figure 39). The basic site is probably composed of a surface $O^{2-}$ anion, as shown in Figure 17. This is an important issue, that an acidic site acts as an anchor point of the position-4 OH group of 1,4-butanediol. Comparing $CO_2$ with $NH_3$, the poisoning effect of $CO_2$ is strong: both the conversion and the selectivity to unsaturated alcohols in $CO_2$ flow are much lower than those in a $NH_3$ carrier. These results indicate that both basic and acidic sites participate in the formation of 3-buten-1-ol via an acid–base concerted mechanism. In particular, basic sites, together with the tridentate coordination, would play the main role of the dehydration.

The dehydration of 1,3-butanediol over $Er_2O_3$ and $CeO_2$ is also inhibited under $CO_2$ and $NH_3$ flow conditions at 275 °C.[43] The degree of poisoning on $CeO_2$ is smaller than that on $Er_2O_3$. Especially, $CO_2$ does not effectively work as a poison at 325 °C. This is a significant difference between $Er_2O_3$ and $CeO_2$. The reaction mechanism over $CeO_2$ is different from that over $Er_2O_3$. It is explained in that the dehydration of 1,3-butanediol proceeds by the $Ce^{4+}$–$Ce^{3+}$ redox of $CeO_2$ in Figure 38. In other words, the difference is whether the basic $O^{2-}$ anion is contributed to the abstraction of hydrogen of methylene group (Figure 39).

## 7. DEHYDRATION OF 1,4-BUTANEDIOL OVER $ER_2O_3$ NANORODS

Recently, a number of research groups have reported the preparation of metal oxide nanorods, such as $MnO_2$,[70] NiO,[71] and $Fe_2O_3$.[72] Nanorods are often prepared by hydrothermal treatment methods. In hydrothermal methods, carboxylic acids, amines, and surfactants are often added in the mixture of the precursor. It is well-known that rare earth oxides with a cubic phase, such as $CeO_2$ and $Er_2O_3$, generally consist of spherical or octahedral nanocrystals, which are usually called nanoparticles. In contrast, $CeO_2$ nanocrystals with unusual shapes, such as nanorods,[73–75] nanocubes,[74] and nanoplates,[75] have been prepared under hydrothermal conditions. The nanocrystals expose specific crystal facets on the surface. For example, $CeO_2$ nanorods mainly expose both {220} and {200} facets on the surface, and $CeO_2$ nanocubes expose only the {200} facet, whereas $CeO_2$ nanoparticles mainly expose the {111} facet.[73,74] Although the additives might work as a crystal growth inhibitor, nanorods are obtained even without an organic additive.[75] $Er_2O_3$ nanorods are also prepared under hydrothermal[76] and supercritical $CO_2$[77] conditions. In the nanorod preparation, alkaline hydroxides are used mostly as a precipitation reagent, and the residual metal cations as well as organic additives sometimes work as a catalyst poison.

Mai et al. have prepared three types of $CeO_2$ nanomaterials—nanopolyhedron, nanorod, and nanocube—and have investigated CO oxidation over the materials.[74] The nanomaterials of $CeO_2$ expose different crystal planes: the nanopolyhedron exposes mainly {111} and {200} facets, and nanorod exposes {220} and {200} facets. The nanocube exposes mostly the {200} facet. The oxygen storage capacity (OSC) measured by CO oxidation depends on the crystal facets of $CeO_2$: OSC values of $CeO_2$ nanorods and nanocubes are twice as high as that of nanopolyhedrons. CO oxidation over $CeO_2$ is categorized to be a crystal-surface-sensitive reaction.

We have successfully prepared $Er_2O_3$ nanorods using an aqueous ammonia solution as a precipitation reagent without organic additives, such as surfactant, fatty acid, or alcohol.[78] The $Er_2O_3$ nanorods are obtained at an appropriate pH under hydrothermal conditions at temperatures higher than 100 °C, for long reaction times, or both. $Er_2O_3$ nanorods exposed mainly {440} and {400} facets on the surface (Figure 40).

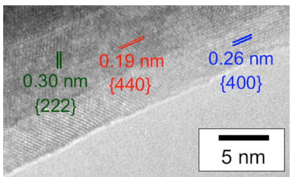


**Figure 40.** High-resolution TEM image of $Er_2O_3$ nanorods prepared under hydrothermal conditions at 200 °C for 24h. Republished with permission from ref 78.

$Er_2O_3$ nanorods showed excellent catalytic activity compared with commercial $Er_2O_3$ nanoparticles in the dehydration of 1,4-butanediol to produce 3-buten-1-ol (Figure 41). The catalytic activity of $Er_2O_3$ nanorods clearly indicates that the active sites exist on either {440} or {400} facets.

## 8. CONCLUSIONS AND PERSPECTIVES

Vapor-phase catalytic dehydration of alkanediol to produce unsaturated alcohols over rare earth oxides was reviewed. $CeO_2$ effectively catalyzed the dehydration of 1,3-butanediol to produce 3-buten-2-ol and *trans*-2-buten-1-ol. In the dehydration of 1,4-butanediol, heavy rare earth oxides, such as $Er_2O_3$, $Yb_2O_3$, and $Lu_2O_3$, selectively catalyzed the formation of 3-buten-1-ol. In the dehydration of 1,5-pentanediol, $Yb_2O_3$, $Lu_2O_3$, and $Sc_{0.5}Yb_{1.5}O_3$ catalysts efficiently worked to produce 4-penten-1-ol. The active and selective oxides were composed


dx.doi.org/10.1021/cs300781v | ACS Catal. 2013, 3, 721–734

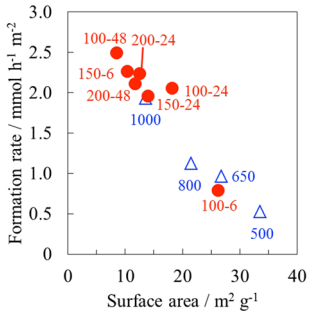


**Figure 41.** Dehydration of 1,4-butanediol over $Er_2O_3$ catalysts with (solid circle, numbers indicate hydrothermal temperature and duration) nanorods and (open triangle, number indicates calcination temperature) nanoparticles. Republished with permission from ref 78.

of large particles with well-crystallized fluorite or bixbyite structure. Small oxide particles with poor crystallinity decreased the selectivity to unsaturated alcohols because of their dehydrogenation ability. Calcination at high temperatures and hydrothermal treatment were efficient in the preparation of selective rare earth oxide catalysts. In the reactions of different alkanediols, the reactivity of alkanediols was dependent on the length between the OH groups as well as on the catalysts. Quantum calculations revealed the probable reaction mechanism in the dehydration of 1,3-butanediol: 1,3-butanediol was adsorbed on the $O^{2-}$ defect site with tridentate coordination where the OH groups and H of position-2 methylene were interacted with surface $Ce^{4+}$ cations, etc. in the activated adsorption of alkanediols in the formation of unsaturated alcohols. The abstraction of the position-2 H by $Ce^{4+}$ was the initial step of 1,3-butanediol dehydration in the formation of unsaturated alcohols. Monoalcohols had adsorption energies smaller than that of 1,3-butanediol so that the product unsaturated monoalcohols were not reactants in the presence of 1,3-butanediol in the vapor phase.

We habitually think catalyst materials must have sufficient catalyst life as well as high activity and high selectivity. Fortunately, most bixbyite oxides are preferable in the dehydration of alkanediols. Other than the rare earth oxides, monoclinic $ZrO_2$ and $In_2O_3$ show catalytic activities similar to those of rare earth oxides, whereas $In_2O_3$ is deactivated in the dehydration of 1,3-propanediol and 1,3-butanediol in the initial reaction period.[29] High selectivity to unsaturated alcohols can be realized on large oxide particles with high crystallinity. Small particles with low crystallinity have different facets with vacancy, step, and kink structures, which could catalyze side reactions to reduce the selectivity to the major product.

We had fortunately used $CeO_2$ with specific surface areas of, at most, 20 $m^2\ g^{-1}$ in the first report of selective formation of unsaturated alcohols,[17] and later found $CeO_2$ with high surface area catalyzed side reactions, such as dehydrogenation.[27,42] We were faced with the unusual phenomenon that high-surface-area catalysts are not selective. It was serendipitous to discover the importance of the crystallinity of the catalyst to the selectivity to target products.

Shimizu et al. have recently reported pure $CeO_2$-catalyzed reactions of nitriles and amides with nucleophiles, such as $H_2O$, alcohols, and amines.[79] Selective formation of amides, ester, and *N*-alkylamides from nitriles is catalyzed by $CeO_2$ under aqueous or solvent-free conditions. They suggest that a cooperation of a Lewis acid site ($Ce^{4+}$ cation) and an acid–base (Ce–O) pair site plays an essential role in the catalytic reaction mechanism, and they proved the presence of acidic sites by IR measurement of adsorbed pyridine.[80] Acid–base concerted mechanisms, whose either acidity or basicity is as weak as an unmeasurable level of the strength, could be important for other selective reactions.

$ZrO_2$ shows Hofmann elimination character: it catalyzes selective formation of 1-butene with a small amount of 2-butene in the dehydration of 2-butanol.[81] The feature quite resembles those of rare earth oxides.[44−47] Rare earth oxides are as expensive as noble metals, so it is required their usage in catalyst be reduced. In the dehydration of 1,4-butanediol, monoclinic $ZrO_2$ is actually the most suitable support for rare earth oxides.[62] Therefore, $ZrO_2$-supported rare earth oxide catalysts must be an alternative to pure rare earth oxides.

Spectroscopies such as IR, XPS, and XAFS for the analysis of surface properties are effective and important to discuss the surface structure of catalysts. However, reaction mechanisms are not always discussed by the spectroscopic data. Density functional theory (DFT) calculation has been expected as a "microscope" available to observe the atomic and electronic details of materials.[82] The combination of DFT with paired interacting orbital (PIO) calculation[51] is a powerful tool as a microscope, which we would like to call "calculation microscope", to examine the reaction mechanism. To clarify the mechanism, as shown in the dehydration of 1,3-butanediol over $CeO_2$ (Section 6.1), we additionally visualized the reaction mechanism by preparing an animation (displayed in the Supporting Information) of the dehydration of 1,3-butanediol over the {222} facet of a bixbyite oxide, such as $Er_2O_3$. In addition, we will report the calculation results of the acid–base concerted mechanism (Figure 39) in the dehydration of 1,4-butanediol over bixbyite-type rare earth oxide catalysts in the near future.

There still remain several questions. Additive cations are expected to be modifiers for a mixed oxide such as $Sc_{2-x}Yb_xO_3$ (Section 5.3). Ionic radius related to the geometry of surface, i.e. distance between the surface cations must affect the catalytic performance (Figure 29). $Er_2O_3$ nanorods have different facets on the surface (Section 7). Which facet of {222}, {440}, or {400} is the most active on the bixbyite surface? Oxide nanocrystals possess a high possibility to solve the question. The smooth surface of a specific facet should provide a unique catalytic activity. We have tried to prepare bixbyite nanocubes with only {400} facet, which is expected to clarify the intrinsic catalytic activity of the {400} facet. Development of novel catalyst preparation methods is expected to promote obtaining catalyst materials with specific smooth surfaces. $ZrO_2$ and $In_2O_3$ as well as rare earth oxides with similar crystal structures can be used as a matrix or additives to produce binary oxides, which are expected to be novel catalysts with specific selectivities. We would like to elucidate the true active site on the active oxides.

## ■ ASSOCIATED CONTENT

### Supporting Information

A speculative animation for the dehydration of 1,3-butanediol over the {222} facet of bixbyite oxide. This material is available free of charge via the Internet at http://pubs.acs.org.

## ■ AUTHOR INFORMATION

### Corresponding Author

*E-mail: satoshi@faculty.chiba-u.jp.

## Notes

The authors declare no competing financial interest.

## ■ ACKNOWLEDGMENTS

Our research work has been supported in part by a Grant-in-Aid for Scientific Research B (16360398) from the Japan Society for the Promotion of Science.

## ■ REFERENCES

(1) Brace, N. O. *J. Am. Chem. Soc.* **1955**, *77*, 4666−4668.
(2) Heinemann, C.; Jautelat, M.; Kuhn, O.; Goossen, L. J.; Ganzer, D. DE Patent 10064751, 2002.
(3) Nagareda, K.; Suzuki, S. JP Patent 3523360, 2004.
(4) Nagareda, K.; Yoshimura, N. JP Patent 3563105, 2004.
(5) Tsuji, J.; Shimizu, I.; Minami, I. *Chem. Lett.* **1984**, *6*, 1017−1020.
(6) Falling, S. N. U.S. Patent Appl. Publ. 20040171892, 2004.
(7) Falling, S. N. U.S. Patent 5406007, 1995.
(8) Konishi, M.; Matsufuji, K. JP Patent Publ. 2007-302639, 2007.
(9) Grosselin, J.-M.; Mercier, C. FR Patent 8716627, 1987.
(10) Inoue, Y.; Nishiyama, H.; Saito, N. JP patent 4862162, 2011.
(11) Kaneda, K.; Mizugaki, T. *Organometallics* **1996**, *15*, 3247−3249.
(12) Mäki-Arvela, P.; Hájek, J.; Salmi, T.; Murzin, D. Y. *Appl. Catal., A* **2005**, *292*, 1−49.
(13) Rodiansono, Hara, T.; Ichikuni, N.; Shimazu, S. *Chem. Lett.* **2012**, *41*, 769−771.
(14) Oku, T.; Yoshida, Y. JP Patent Publ. 2009-107949, 2009.
(15) Yamanaka, T.; Imai, T. *Bull. Chem. Soc. Jpn.* **1981**, *54*, 1585−1586.
(16) Ichikawa, N.; Sato, S.; Takahashi, R.; Sodesawa, T. *J. Mol. Catal. A: Chem.* **2006**, *256*, 106−112.
(17) Sato, S.; Takahashi, R.; Sodesawa, T.; Honda, N.; Shimizu, H. *Catal. Commun.* **2003**, *4*, 77−81.
(18) Sato, S.; Takahashi, R.; Sodesawa, T.; Yamamoto, N. *Catal. Commun.* **2004**, *5*, 397−400.
(19) Yamamoto, N.; Sato, S.; Takahashi, R.; Inui, K. *Catal. Commun.* **2005**, *6*, 480−484.
(20) Vaidya, S. H.; Bhandari, V. M.; Chaudhari, R. V. *Appl. Catal., A* **2003**, *242*, 321−328.
(21) Baba, T.; Ono, Y. *J. Mol. Catal.* **1986**, *37*, 317−326.
(22) Ichikawa, N.; Sato, S.; Takahashi, R.; Sodesawa, T.; Inui, K. *J. Mol. Catal. A: Chem.* **2004**, *212*, 197−203.
(23) Adachi, G.; Imanaka, N. *Chem. Rev.* **1998**, *98*, 1479−1514.
(24) Sato, S.; Takahashi, R.; Kobune, M.; Gotoh, H. *Appl. Catal., A* **2009**, *356*, 57−63.
(25) Shanon, R. D. *Acta Crystallogr., A* **1976**, *32*, 751−767.
(26) Wang, Z. L.; Feng, X. *J. Phys. Chem. B* **2003**, *107*, 13563−13566.
(27) Igarashi, A.; Ichikawa, N.; Sato, S.; Takahashi, R.; Sodesawa, T. *Appl. Catal., A* **2006**, *300*, 50−57.
(28) Kobune, M.; Sato, S.; Takahashi, R. *J. Mol. Catal. A: Chem.* **2008**, *279*, 10−19.
(29) Tsunekawa, S.; Fukuda, T.; Kasuya, A. *Surf. Sci.* **2000**, *457*, L437−L440.
(30) Nörenberg, H.; Briggs, G. A. D. *Surf. Sci.* **1999**, *424*, L352−L355.
(31) Fukui, K.; Namai, Y.; Iwasawa, Y. *Appl. Surf. Sci.* **2002**, *188*, 252−256.
(32) Namai, Y.; Fukui, K.; Iwasawa, Y. *Catal. Today* **2003**, *85*, 79−91.
(33) Namai, Y.; Fukui, K.; Iwasawa, Y. *J. Phys. Chem. B* **2003**, *107*, 11666−11673.
(34) Esch, F.; Fabris, S.; Zhou, L.; Montini, T.; Africh, C.; Fornasiero, P.; Comelli, G.; Rosei, R. *Science* **2005**, *309*, 752−755.
(35) Kosacki, I.; Suzuki, T.; Anderson, H. U.; Colomban, P. *Solid State Ionics* **2002**, *149*, 99−105.
(36) Nörenberg, H.; Briggs, G. A. D. *Surf. Sci.* **1998**, *402−404*, 734−737.
(37) Rosynek, M. P. Catal. *Rev. Sci. Eng.* **1977**, *16*, 111−154.
(38) Adachi, G.; Imanaka, N.; Kang, Z. C. *Binary Rare Earth Oxides*: Kluwer Academic Publishers: Dordrecht, 2004.
(39) Segawa, M.; Sato, S.; Kobune, M.; Sodesawa, T.; Kojima, T.; Nishiyama, S.; Ishizawa, N. *J. Mol. Catal. A: Chem.* **2009**, *310*, 166−173.
(40) Takahashi, R.; Yamada, I.; Iwata, A.; Kurahashi, N.; Yoshida, S.; Sato, S. *Appl. Catal., A* **2010**, *383*, 134−140.
(41) Sato, S.; Takahashi, R.; Sodesawa, T.; Honda, N. *J. Mol. Catal. A: Chem.* **2004**, *221*, 177−183.
(42) Igarashi, A.; Ichikawa, N.; Sato, S.; Takahashi, R.; Sodesawa, T. *Appl. Catal., A* **2006**, *314*, 134.
(43) Gotoh, H.; Yamada, Y.; Sato, S. *Appl. Catal., A* **2010**, *377*, 92−98.
(44) Kahn, A. P.; Harris, S. H. U.S. Patent 7259280 B1, 2007.
(45) Yoshida, Y.; Arai, Y.; Kado, S.; Kunimori, K.; Tomishige, K. *Catal. Today* **2006**, *115*, 95−101.
(46) He, Y.; Li, Q.; Wang, Y.; Zhao, Y. *Chin. J. Catal.* **2010**, *31*, 619−622.
(47) Sato, S.; Takahashi, R.; Yamamoto, N.; Kaneko, E.; Inoue, H. *Appl. Catal., A* **2008**, *334*, 84−91.
(48) Akashi, T.; Sato, S.; Takahashi, R.; Sodesawa, T.; Inui, K. *Catal. Commun.* **2003**, *4*, 411−416.
(49) Sato, S.; Takahashi, R.; Sodesawa, T.; Igarashi, A.; Inoue, H. *Appl. Catal., A* **2007**, *328*, 109−116.
(50) Nozawa, T.; Sato, S.; Takahashi, R. *Top. Catal.* **2009**, *52*, 609−617.
(51) Sato, S.; Takahashi, R.; Kobune, M.; Inoue, H.; Izawa, Y.; Ohno, H.; Takahashi, K. *Appl. Catal., A* **2009**, *356*, 64−71.
(52) Igarashi, A.; Sato, S.; Takahashi, R.; Sodesawa, T.; Kobune, M. *Catal. Commun.* **2007**, *8*, 807−810.
(53) Yamamoto, N.; Sato, S.; Takahashi, R.; Inui, K. *J. Mol. Catal. A: Chem.* **2006**, *243*, 52−59.
(54) Inoue, H.; Sato, S.; Takahashi, R.; Izawa, Y.; Ohno, H.; Takahashi, K. *Appl. Catal., A* **2009**, *352*, 66−73.
(55) Sato, F.; Okazaki, H.; Sato, S. *Appl. Catal., A* **2012**, *419−420*, 41−48.
(56) Galceran, M.; Pujol, M. C.; Carvajal, J. J.; Mateos, X.; Zaldo, C.; Aguiló, M.; Díaz, F. *J. Lumin.* **2010**, *130*, 1437−1443.
(57) Sato, F.; Sato, S. *Catal. Commun.* **2012**, *27*, 129−133.
(58) Abe, K.; Ohishi, Y.; Okada, T.; Yamada, Y.; Sato, S. *Catal. Today* **2011**, *164*, 419−424.
(59) Tanabe, K.; Misono, M.; Ono, Y.; Hattori, H. *New Solid Acids and Bases*: Tokyo, 1989, pp 260−267.
(60) Lundeen, A. J.; Hoozer, R. V. *J. Org. Chem.* **1967**, *32*, 3386−3389.
(61) Bernal, S.; Trillo, J. M. *J. Catal.* **1980**, *66*, 184−190.
(62) Davis, B. H.; Russell, S. N.; Reucroft, P. J.; Shalvoy, R. B. *J. Chem. Soc., Faraday Trans.* **1980**, *I 76*, 1917−1922.
(63) Sato, S.; Takahashi, R.; Sodesawa, T.; Matsumoto, K.; Kamimura, Y. *J. Catal.* **1999**, *184*, 180−188.
(64) Kamimura, Y.; Sato, S.; Takahashi, R.; Sodesawa, T.; Akashi, T. *Appl. Catal., A* **2003**, *252*, 399−410.
(65) Ichikawa, N.; Sato, S.; Takahashi, R.; Sodesawa, T. *J. Mol. Catal. A: Chem.* **2005**, *231*, 181−189.
(66) Ichikawa, N.; Sato, S.; Takahashi, R.; Sodesawa, T.; Fujita, H.; Atoguchi, T.; Shiga, A. *J. Catal.* **2006**, *239*, 13−22.
(67) Pines, H.; Manassen, J. *Adv. Catal.* **1996**, *16*, 49−93.
(68) Setoyama, T. *Catal. Today* **2006**, *116*, 250−262.
(69) Kumar, V. S.; Nagaraja, B. M.; Shashikala, V.; Seetharamulu, P.; Padmasri, A. H.; Raju, B. D.; Rao, K. S. R. *J. Mol. Catal. A: Chem.* **2004**, *223*, 283−288.
(70) Wang, X.; Li, Y. *Chem. Commun.* **2002**, 764−765.
(71) Liang, J.; Li, Y. *Chem. Lett.* **2003**, *32*, 1126−1127.
(72) Zeng, S.; Tang, K.; Li, T. J. *Colloid Interface Sci.* **2007**, *312*, 513−521.
(73) Zhou, K.; Wang, X.; Sun, X.; Peng, Q.; Li, Y. *J. Catal.* **2005**, *229*, 206−212.
(74) Mai, H.-X.; Sun, L.-D.; Zhang, Y.-W.; Si, R.; Feng, W.; Zhang, H.-P.; Liu, H.-C.; Yan, C.-H. *J. Phys. Chem. B* **2005**, *109*, 24380−24385.

(75) Pan, C.; Zhang, D.; Shi, L. *J. Solid State Chem.* **2008**, *181*, 1298−1306.
(76) Wang, X.; Li, Y. *Angew. Chem., Int. Ed.* **2002**, *41*, 4790−4793.
(77) Assaaoudi, H.; Fang, Z.; Barralet, J. E.; Wright, A. J.; Butler, I. S.; Kozinski, J. A. *Nanotechnology* **2007**, *18*, 445606−1−7.
(78) Sato, F.; Yamada, Y.; Sato, S. *Chem. Lett.* **2012**, *41*, 593−594.
(79) Tamura, M.; Shimizu, K.; Satsuma, A. *Chem. Lett.* **2012**, *41*, 1397−1405.
(80) Tamura, M.; Shimizu, K.; Satsuma, A. *Appl. Catal., A* **2012**, *433*−*434*, 145.
(81) Yamaguchi, T.; Sasaki, H.; Tanabe, K. *Chem. Lett.* **1973**, *2*, 1017−1018.
(82) Hafner, J.; Wolverton, C.; Ceder, G. *MRS Bull.* **2006**, *31*, 659−668.